Szczyglowski, C. P., Neild, S., Titurus, B., & Jiang, J. Z. (2018). Passive Gust Load Alleviation in a Truss-Braced Wing Using an Inerter-Based Device. In *AIAA/ASCE/AHS/ASC Structures, Structural Dynamics, and Materials Conference, AIAA SciTech Forum* [AIAA 2018-1958] (Journal of Aircraft). American Institute of Aeronautics and Astronautics Inc. (AIAA). https://doi.org/10.2514/6.2018-1958

Peer reviewed version

Passive Gust Load Alleviation In a Truss-Braced Wing Using an Inerter-Based Device

Christopher P. Szczyglowski,* Simon A. Neild†, Brano Titurus‡ and Jason Z. Jiang§
Faculty of Engineering, University of Bristol, Bristol, BS8 1TR, United Kingdom

Etienne Coetzee¶
Airbus, Filton, Bristol, BS34 7PA, United Kingdom

This paper presents a novel method for gust loads alleviation in a truss-braced wing in which an inerter-based device located in the truss structure is used to reduce peak-loads during a discrete "1-cosine" gust. Recent studies have shown that gust loads and flutter are critical to the wing sizing and the overall performance of the truss-braced wing concept and it is understood that without additional efforts to mitigate against these effects the benefits of the truss-braced wing concept may be significantly reduced. It is demonstrated that the use of a tunable device known as a tuned inerter damper allows specific vibration modes to be targeted during the gust response, resulting in a reduction of 25% in root bending moment and 5% in root torque when tuned to the second global wing bending mode. Furthermore, it is noted that the force coefficients of the tuned inerter damper are small in comparison with the pure damper device and could be feasible within the scope of an aerospace application.

I. Nomenclature

A_0, A_1, A_2	=	transfer function coefficients for the dependent degree of freedom
B_0, B_1, B_2	=	transfer function coefficients for the independent degree of freedom
b	=	inertance
c	=	viscous damping coefficient
e	=	MSC.Nastran EPOINT
f_1, f_2	=	force at terminal 1 and terminal 2 of the vibration suppression device
F_g	=	flight profile alleviation factor
H	=	gust gradient
k	=	spring stiffness
p	=	Laplace variable
s	=	MSC.Nastran SPOINT
u_d	=	transfer function dependent degree of freedom
U_{ds}	=	gust design velocity
u_i	=	transfer function independent degree of freedom
U_{ref}	=	reference gust velocity
V	=	aircraft forward speed
w_g	=	vertical gust velocity
x_1, x_2	=	displacement at terminal 1 and terminal 2 of the vibration suppression device
$\dot{x}_1, \dot{x}_2$	=	velocity at terminal 1 and terminal 2 of the vibration suppression device
$\ddot{x}_1, \ddot{x}_2$	=	acceleration at terminal 1 and terminal 2 of the vibration suppression device
Y	=	generic transfer function
ϕ	=	modal coordinate
ω	=	tuning frequency of the vibration suppression device

*Postgraduate Student, Department of Aerospace Engineering, Queen's Building, University Walk, Bristol, BS8 1TR
†Professor of Nonlinear Structural Dynamics, Department of Mechanical Engineering
‡Senior Lecturer in Aerospace Dynamics, Department of Aerospace Engineering
§Lecturer in Dynamics and Control, Department of Mechanical Engineering
¶Future Projects Engineer, Future Project Office, Airbus Operations Ltd., Pegasus House Aerospace Avenue Filton, Bristol, BS34 7PA

II. Introduction

In recent years an increased level of research has been devoted to the study of more energy efficient aircraft that will meet the environmental performance improvements set out in initiatives such as Vision 2020 and Flight Path 2050. Some of these studies have considered the implementation of a new aircraft concept that can provide significant improvements in overall aircraft efficiency and noise[1].

The truss-braced wing (TBW) concept offers an exciting alternative to the cantilever wing design as the addition of the truss structure creates a structurally efficient design which reduces the spanwise bending moments and torques inboard of the strut[2, 3]. This enables the inboard portion of the wing to be designed with a reduced thickness-to-chord ratio providing a reduction in wing weight as well as lower wave and profile drag. Furthermore, the reduced bending moment allows a larger wingspan to be achieved resulting in an increased aspect ratio and a reduction in induced drag. Multidisciplinary optimisation studies [4, 5] have shown that a truss-braced wing design has a lower sweep angle than a cantilever wing. This leads to a reduction in spawise crossflow[6] thus promoting more laminar flow and hence lower friction drag, however it should be noted that the interference drag from the truss-structure can have a detrimental effect on performance if it is not properly designed[7, 8]. Even with the effects of the truss interference drag taken into account, numerous studies have shown that the truss-braced wing concept can provide an overall improvement in maximum take-off weight and fuel burn compared to a traditional cantilever design [4, 5, 9].

A recent study by Malik *et al.*[10] showed that aeroelastic phenomena such as flutter are the main constraints which drive the overall design of the TBW aircraft, thereby placing a limit on the practical efficiency savings that can be achieved when considering a braced wing design. Furthermore, initial sizing studies conducted as part of the NASA and Boeing Subsonic Ultra Green Aircraft Research (SUGAR)[11] project have shown that gust loads are responsible for sizing many of the structural components in the wing box[12]. Hence, a primary requirement for the success of the TBW concept is to reduce the effect of these aeroelastic phenomena, thus enabling further reductions in wing weight and an enhancement of overall efficiency.

A typical strategy to reduce gust loads is to operate aerodynamic control surfaces using control laws in order to modify the wing aerodynamic forces in such a way that the wing gust response is minimised [13]. This approach is commonplace across the aerospace industry and has been applied to the SUGAR TBW aircraft during aeroelastic wind tunnel tests where it was observed to suppress flutter and provide some gust load alleviation[14]. Other methods of loads alleviation have been proposed such as folding wing tips[15], aeroelastic tailoring[16] and morphing structures[17].

In this paper an alternative approach to loads alleviation in a truss-braced wing is presented. This is to use a passive vibration absorber located in the truss structure to reduce the gust response. Such an approach is not feasible in a cantilever wing as a location does not exist where the relative motion of the wing structure can be exploited by a two terminal device. The addition of a strut means that there are now several candidate locations where a device could be placed in order to provide loads relief. For example, if a hinge connection between the strut and the wing is employed then the rotation of the strut about that joint could be utilised or the jury-strut may experience significant relative motion due to the combined bending of the wing and the primary strut.

Vibration absorbers are common in many structures which undergo large motions or are subject to vibrations which are detrimental to the overall performance or health of the structure. Typically these absorbers are restricted to a

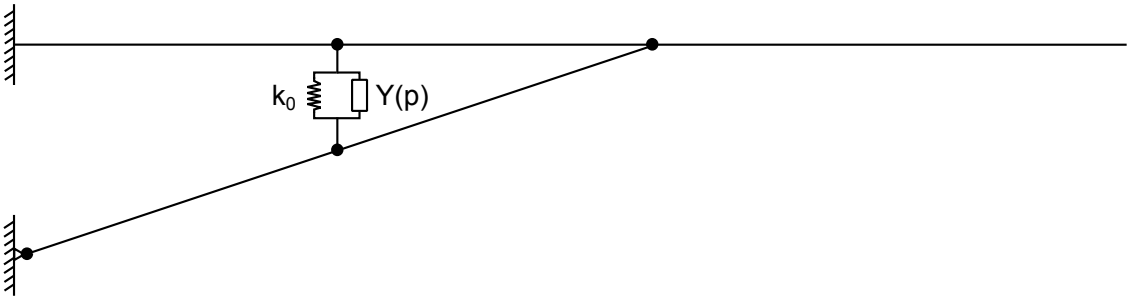

Fig. 1 Schematic of the TBW with the jury strut modelled as a spring with a generic transfer function in parallel.

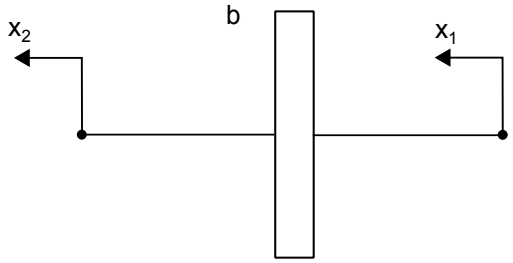

Fig. 2 The inerter element

combination of spring and damper elements and lumped masses[18] in order to suppress the motion of the structure. However, in 2002 Smith [19] introduced a mechanical element known as an inerter that is now being used extensively in the field of mechanical networks. An inerter is a mechanical two-terminal element with the property that the applied force at the terminals is proportional to the relative acceleration across the terminals, i.e. $F = b(\ddot{x_1} - \ddot{x_2})$, where, using the notation of Fig. 2, b is the inertance and $\ddot{x_1}$ and $\ddot{x_2}$ are the accelerations at the terminals of the device.

The introduction of the inerter element provided a complete analogy between electrical and mechanical systems and fundamentally enhanced the range of vibration suppression controllers that can be achieved using passive mecahnical devices.[20]. In recent years inerter-based devices have been identified for a wide-range of applications including the automotive[21], locamotive[22, 23] and civil engineering industries[24, 25]. Furthermore, inerter-based devices have been proposed to suppress shimmy [26] and improve touch down performance [27] in aircraft landing gear. Inerter-based devices are particularly useful in aerospace applications as the inertance b can be much larger than the actual mass of the device via the use of gearing mechanisms[19].

In this study a truss-braced wing model based on the NASA/Boeing SUGAR VOLT concept aircraft[12] is augmented with a vibration suppression device in parallel with the jury-strut, as in Fig. 1, in order to provide loads relief during a discrete "1-minus cosine" gust. The *structure-based* approach to mechanical network design[28] is utilised with two candidate device layouts considered, these are a damper and a tuned inerter damper[24]. An outline of mechanical network design is provided in section III C. MSC.Nastran is used to determine the gust response of the aeroelastic model and the performance of each device layout is examined across a range of gust cases to identify appropriate values for the force coefficients of the different mechanical elements in the device. (e.g. spring stiffness, viscous damping coefficient and inertance)

This paper begins with a description of the aeroelastic model and the methodology for designing a vibration suppression device, as well as a note on the modelling method of the device in MSC.Nastran. Next, the baseline gust response of the truss-braced wing model is presented, with specific emphasis on the gust loads envelope and the structural modes which are most active throughout the gusts. In section V the various vibration suppression devices are included in the model and their effect on the gust loads envelope is observed for a range of parameter values. Finally, the main findings of the study are discussed and conclusions are presented in the final section along with suggestions for further work.

III. Methodology

In this section the truss-braced wing aeroelastic model is described and the key points regarding the structural and aerodynamic modelling are discussed. The different methodologies for designing mechanical networks are introduced and the method for modelling the device is outlined.

A. Finite Element Model

The half-wing model is based on the 765-09 Rev. D version of the SUGAR Volt concept aircraft[12] and the planform and truss topology are taken directly from Table 2.29 - 2.31 and Fig. 2.155 - 2.157 of the SUGAR report[12]. It is important to note that the primary strut of the 765-09 Rev. D model is offset from the beam line towards the front spar, however there is no offset for the jury-strut element. Having an offset strut provides a passive loads alleviation benefit for the wing torque as moment arm of the strut axial load allows a moment to be imparted onto the wing which reduces the twist angle. [2]

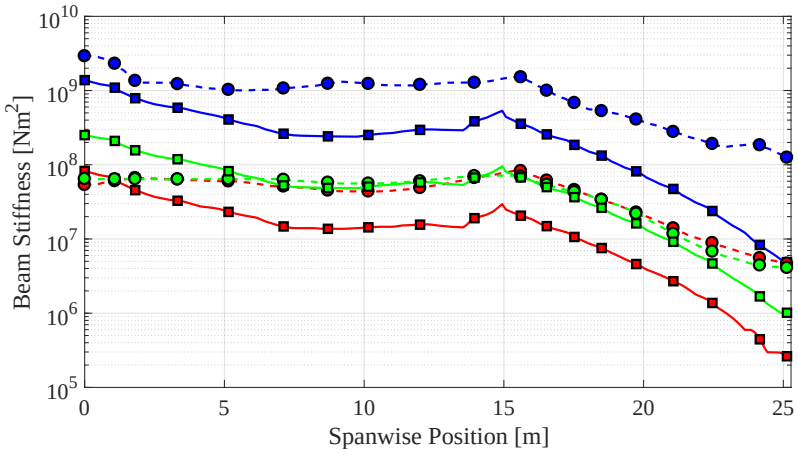

(a) Wing Beam Stiffness

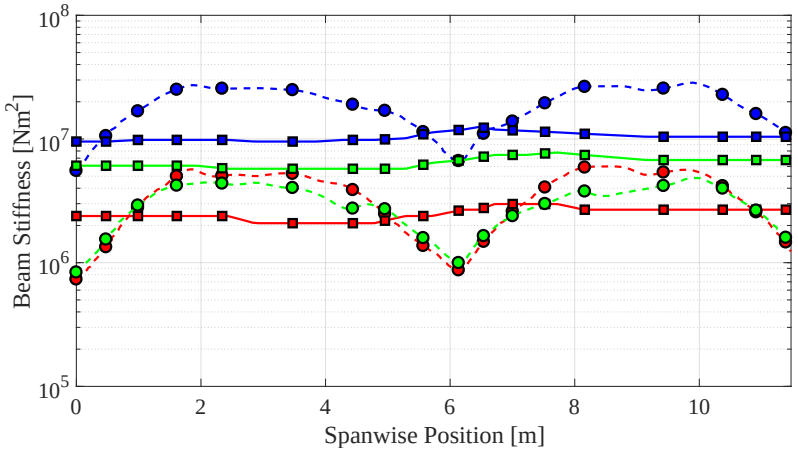

(b) Strut Beam Stiffness

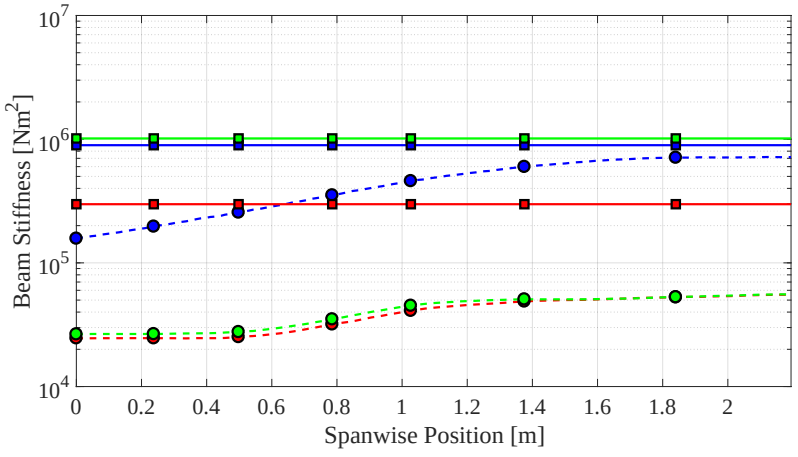

(c) Jury-Strut Beam Stiffness

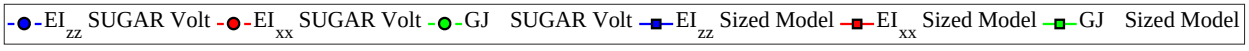

Fig. 3 Beam Stiffness comparison between the SUGAR Volt 765-09 Rev. D aircraft and the sized wing model.

As the mass and stiffness information is not published in full in these reports a sizing routine[29] based on the Fully Stressed Design (FSD) criteria has been used to generate mass and stiffness distributions for the wing, strut and jury-strut. The sized wing model is fundamentally different to the 765-09 Rev. D and therefore the underlying aeroelastic behaviour examined in this study should not be taken as indicative of the SUGAR Volt model.

Figure 3 shows a comparison of the beam stiffness for the wing beam elements. As the sizing routine utilises a quasi-isotropic material based on the Hart-Smith 10%[30] rule for composites the resulting structure is lighter and more flexible than the SUGAR model which uses an advanced black metal. The exception to this is the jury-strut element which is significantly stiffer.

This is due to the poor buckling performance of the truss structure as the strut geometry of the sized wing model does not have the same distinctive 'bow-tie' chord distribution as the SUGAR model which has been specifically designed to alleviate buckling in the truss members. Furthermore, the FSD is known to provide suboptimum designs for structures with multiple load paths and different material properties[31]. Combining these effects has led to a jury-strut that is significantly oversized when compared to the SUGAR Volt model. The sizing methodology for a TBW is part of ongoing research at the University of Bristol and will be discussed in greater detail in subsequent research.

For the purposes of this study, the jury-strut stiffness has been scaled to match the SUGAR Volt model with the axial stiffness of the beam elements in the 765-09 Rev. D assumed to be one order of magnitude greater than the chordwise bending stiffness EI_{zz} in keeping with the modelling assumptions made by Su[32]. Next, to reduce the complexity of the model and facilitate trade-studies into the effectiveness of the vibration suppression device the jury-strut element is modelled as a linear spring with stiffness $K_0 = EA_{jury}/L_{jury}$ which, for an axial beam stiffness of $1.573 \times 10^6\ N/m^2$ and a length of $2.217\ m$, yields a spring stiffness of $7.1 \times 10^5\ N/m$. Figure 4 shows the aeroelastic model used throughout this study.

B. Aeroelastic Modelling

MSC.Nastran is used to compute the transient gust response of the aeroelastic model as well as determine additional dynamic properties such as modeshapes and associated natural frequencies. For this study the wing reference node is fully-fixed, hence the rigid body modes will not participate in the gust response. This will of course have a significant effect on the participation of the flexible modes, however, as this is a preliminary investigation this simple approach is deemed satisfactory.

The gust loading is idealised as a "1-cosine" gust, the formula for which is taken directly from the certification requirements for large aircraft, Certification Specification 25 (CS-25), as provided by EASA[33].

$$w_g(t) = \frac{U_{ds}}{2}\left[1 - cos(\frac{\pi V t}{H})\right], \tag{1}$$

Here w_g is the gust vertical velocity, H is the gust gradient (distance to reach the peak gust velocity), V is the aircraft forward velocity in TAS and U_{ds} is the gust design velocity, defined as

$$U_{ds} = U_{ref} F_g \left(\frac{H}{106.17}\right)^{\frac{1}{6}}, \tag{2}$$

where F_g is the flight load alleviation factor and U_{ref} is the reference gust velocity in EAS, varied linearly from 13.4m/s EAS at 15,000ft to 7.9m/s EAS at 50,000ft as specified in CS-25. The cruise altitude and Mach number for the 765-09

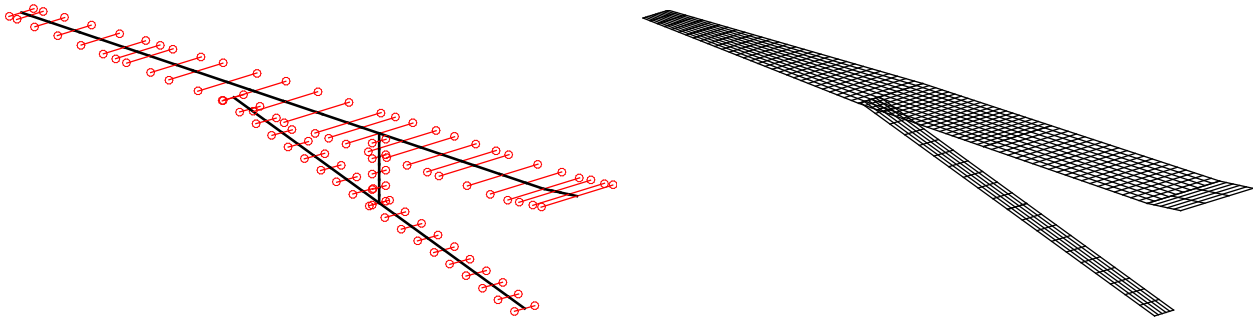

(a) Structural model (b) Aerodynamic model

Fig. 4 Structural and aerodynamic model for the TBW

Rev. D model is given in [12] as 36,000ft and M=0.75 respectively, yielding a gust reference velocity of 10.12m/s EAS and a flight load alleviation factor 0.98.

The aerodynamic forces and moments are calculated using the Double Lattice Method (DLM) provided as part of the aeroelastic solution sequences in MSC.Nastran and a beam spline is used to connect the aerodynamic mesh to the structural grid nodes and transfer all forces and displacements. The doublet lattice method is based on linear unsteady potential flow theory, meaning that the aerodynamic forces are only valid for inviscid, irrotational, incompressible and attached flow, subject to small angles of attack or side-slip. Despite these limitations the DLM aerodynamics are considered to be appropriate in order to obtain an understanding of the general wing response to a discrete gust.

C. Mechanical Network Design

In the field of mechanical network design there are three possible approaches to the design of the network: *structure-based*, *immittance-based* and *structure-immittance*[28].

The *structure-based* approach is the simplest of the three. In this method the layout of the device is initially defined then the parameter values for each element are selected based on certain performance criteria. This allows the complexity of the device as well as how the elements are connected to be tightly controlled, however, the selected layouts are usually sub-optimum compared to those that can be realised by the other two methods.

The *immittance-based* approach is based on finding the optimum device transfer function before the corresponding network layout and element values are determined using network synthesis theory[34]. This is very much the opposite of the *structure-based* approach where the device layout and the related transfer function are predetermined but can lead to complicated layouts. The *immittance-based* approach allows a full range of device layouts with a fixed number of each component type to be explored although it is not possible to place constraints on the parameter values. This can lead to the generation of devices which have an excessive number of elements or parameter values that are not realistic or preferable. The third method, the *structure-immittance* approach[28], allows for the advantages of both of the previous methods.

As this research is concerned with establishing the viability of a vibration suppression device as a method for gust loads alleviation in TBW it is preferable to use the *structure-based* approach. Two device layouts are considered: a viscous damper and a Tuned Inerter Damper (TID)[24]. The TID is analogous to the classical Tuned-Mass-Damper (TMD) with the exception that the mass element is replaced by an inerter as in Fig. 5).

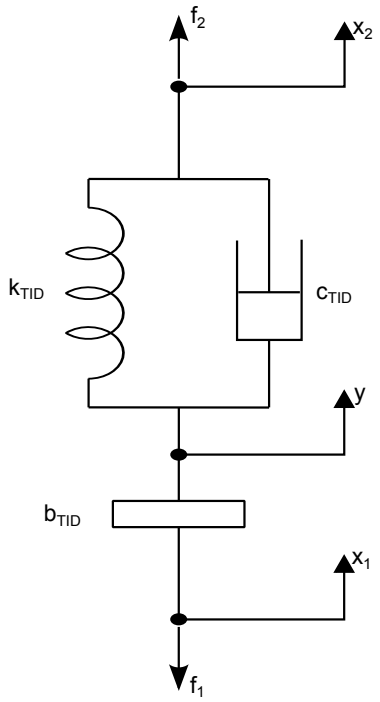

Fig. 5 Schematic of a Tuned-Inerter-Damper (TID)

The advantages of a TID device over the conventional TMD are twofold: Firstly, the use of the inerter element allows a force to be imparted at both terminals of the device, something that is particularly useful for the TBW configuration as it allows for the possibility of a device that can influence multiple parts of the structure. Secondly, the inerter can provide an inertance which is far greater than the mass of the device. For instance, a typical value of the inertance-to-mass ratio is around 40-80, see for example the commercially available device tested in Gonzalez-Buelga *et al.*[35], although devices have been produced with ratios as high as 300[19]. This has obvious benefits in an aerospace application as the weight of the aircraft should be kept to a minimum.

D. Device Modelling

MSC.Nastran has several built-in elements that are capable of modelling scalar and multi-DOF springs and dampers, including the CBUSH element [36] which can model a generalised stiffness and damping relationship between two nodes. However, there does not exist an equivalent element to the inerter, that is to say, an element that generates a force proportional to relative acceleration. Instead MSC.Nastran's built-in transfer function (TF) element must be used to formulate the direct input matrix associated with the dependent and independent degrees of freedom of the inerter. The TF element[36] uses the following equation to define a generic second-order transfer function between a single dependent DOF u_d and an arbitrary number of independent DOFs u_i

$$(B_0 + B_1 p + B_2 p^2)u_d + \sum_i (A_{0_i} + A_{1_i} p + A_{2_i} p^2)u_i = 0, \tag{3}$$

where p is the differential operator d/dt, and the A and B terms are coefficients which, together with p, define the zeros and poles of the transfer function.

This capability can also be used to define more complex device layouts by considering the device as a series of transfer functions chained together, an approach that is made necessary by the fact that the TF element is limited to a second order function. Furthermore, the inputs to the device, such as relative displacement, velocity and acceleration, are themselves defined as Extra Points (EPOINT) or Scalar Points (SPOINT) using Equation 3. Further information can be found in the MSC.Nastran Dynamic Analysis User's Guide[37].

To demonstrate the use of this element the transfer function for the inerter and the tuned-inerter-damper will be derived and related to the terms in Equation 3. Beginning with the inerter element, the force generated by a linear inerter at each terminal of the device is given by

$$f_1 = f_2 = b(\ddot{x}_2 - \ddot{x}_1) = b \times \ddot{e}, \tag{4}$$

where f_i is the force at each terminal, b is the inertance, $\ddot{x}_i$ is the acceleration at each terminal and e is the EPOINT representing the relative displacement between terminals. To implement this relationship in MSC.Nastran the following steps must be taken:

1. Define an EPOINT.
2. Define the device input referencing the EPOINT as the dependent DOF using Equation 3.
3. Define the force at each terminal.*

It is important to note that a transfer function is required to define the force at each terminal of the device, that is to say, a device with only two terminals requires three transfer functions, one for each terminal of the device and one for the EPOINT.†

Considering the TID, the force at the two terminals of the device is

$$f_1 = b(\ddot{y} - \ddot{x}_1), \tag{5}$$

$$f_2 = c(\dot{x}_2 - \dot{y}) + k(x_2 - y), \tag{6}$$

The equation of motion for the intermediate y-DOF can be found by setting the two device forces equal to one another. Converting to the Laplace domain yields

$$Y(p) = \frac{bp^2 X_1(p) + (cp + k)X_2(p)}{bp^2 + cp + k}, \tag{7}$$

*When defining a force or moment acting on a dependent degree of freedom the B terms of the transfer function must be zero.

†The authors realise that it is possible to remove the EPOINT from the transfer function definition and instead use two independent degrees of freedom for each TF element. However, defining the input to the device as an EPOINT allows the relative displacements, velocities and accelerations to be requested as part of the results which is useful for understanding the behaviour of the vibration suppression device.

here, upper case letters denote the Laplace response and p is the Laplace variable in keeping with MSC.Nastran convention for the TF element. Remaining in the Laplace domain, the forces at each terminal of the device are given as

$$F_1(p) = bp^2(Y(p) - X_1(p)), \tag{8}$$

$$F_2(p) = (cp + k)(X_2(p) - Y(p)), \tag{9}$$

The implementation of the TID element in MSC.Nastran is slightly different due to the presence of the intermediate DOF:

1. Define a SPOINT and two EPOINTs.
2. Define the intermediate DOF as a SPOINT using Equation 3.[‡]
3. Using EPOINTs, define the relative quantities for the forces at the device terminals.
4. Define the force at each terminal.

Table 1 shows the transfer function coefficients for the inerter and tuned-inerter-damper as well as the various input quantities. Note that e and s represent EPOINT and SPOINT respectively and subscript 1 and 2 denote the terminals of the device.

Table 1 MSC.Nastran transfer function coefficients for the inerter, tuned-inerter-damper and the device input & output quantities.

	Label	Equation	B_0	B_1	B_2	u_d	A_0	A_1	A_2	u_i
Inerter	Relative quantity between x_1 and x_2	$e_1 = x_2 - x_1$	1	0	0	e_1	1	0	0	x_1
							-1	0	0	x_2
	Force on terminal 1	$f_1 = bp^2 \times e_1$	0	0	0	f_1	0	0	$-b$	e_1
	Force on terminal 2	$f_2 = bp^2 \times e_1$	0	0	0	f_2	0	0	$-b$	e_1
TID	Intermediate DOF	$s = \frac{bp^2x_1+(cp+k)x_2}{bp^2+cp+k}$	k	c	b	s	0	0	$-b$	x_1
							$-k$	$-c$	0	x_2
	Relative quantity between s and x_1	$e_1 = s - x_1$	1	0	0	e_1	1	0	0	x_1
							-1	0	0	s
	Relative quantity between x_2 and s	$e_2 = x_2 - s$	1	0	0	e_2	1	0	0	s
							-1	0	0	x_2
	Force on terminal 1	$f_1 = bp^2 \times e_1$	0	0	0	f_1	0	0	$-b$	e_1
	Force on terminal 2	$f_2 = (cp + k) \times e_2$	0	0	0	f_2	$-k$	$-c$	0	e_2

IV. Gust Response of the Baseline Aeroelastic Model

Before the loads alleviation capability of a vibration suppression device can be studied it is necessary to quantify the gust response of the baseline aeroelastic model without any augmentation. The half-wing model was analysed for a family of ten discrete "1-cosine" gusts with gust gradients in the range 9m to 107m and the maximum and minimum beam loads were extracted for the wing and strut elements. These loads represent the 'extra' loads which the aircraft experiences during a gust in addition to the steady-state loads and henceforth will be referred to as incremental loads. To obtain the complete loads envelope for each component the incremental loads should be added to the steady-state loads which are typically calculated for the 1-g trim condition.

Figure 6 shows the incremental gust loads and the corresponding critical gust gradient for the wing spanwise and torque moments and the strut spanwise bending moment. It is clear from these plots that there is no obvious correlation between gust gradient and peak loads as the critical gusts are distributed throughout the required 9m to 107m range. Although, it should be noted that the 9m gust is not a critical for any of the loads shown in Figure 6 which may be due to the lower power spectral density of the short gusts. If a vibration suppression device is to be used to alleviate gust loads across the whole wing then it is clear that such a device must be effective across a broad spectrum of gust gradients.

[‡]An SPOINT must be used to ensure that the additional mode introduced by the intermediate DOF is added to the a-set matricies before MSC.Nastran conducts the eigenanalysis.

As the unsteady aerodynamic forces are formulated in the frequency domain it is useful to consider which modes are most active throughout the various gusts as this will provide an indication of the modes that contribute to the peak loads. The modal coordinates have been extracted for each mode in the frequency range of interest[§] and the maximum values are plotted against gust gradient in Fig. 7. In total 18 modes were present in this range although many of them have only a small contribution to the overall gust response.

Examining the maximum modal coordinates for the five most active modes reveals that the gust response is dominated by wing bending modes, with the wing wing outboard bending mode showing the most participation throughout the gust spectrum. This result should be expected as the out-of-plane bending stiffness, which is in the spanwise direction, of the wing and strut elements is much lower than the chordwise and torsional stiffness. Furthermore, the strut element is pinned at both ends which promotes the strut spanwise bending mode as there is no stiffness associated with the spanwise bending degree of freedom at the strut root and tip. This suggests that including a device in the structure that can influence these modes will facilitate a decrease in incremental gust loads.

Interestingly, the response of mode 1, mode 2 and mode 8 has not reached a maximum inside the defined gust spectrum which may indicate that additional gust gradients should be considered when finding the gust loads envelope.

[§]Solution frequencies were defined in the range 0Hz to 30Hz with a frequency increment $\Delta F = 0.005$Hz.

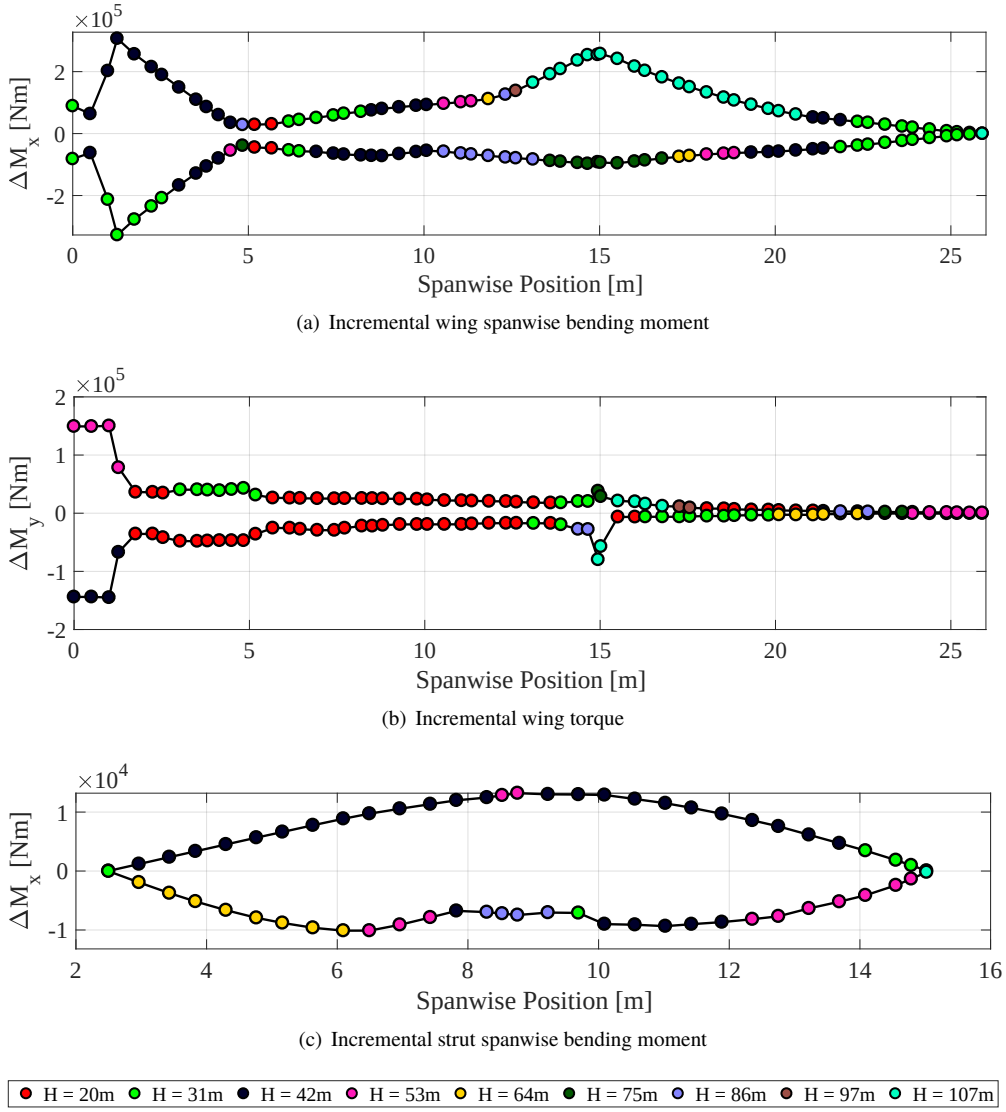

Fig. 6 Loads envelopes for the wing and strut for the baseline aeroelastic model

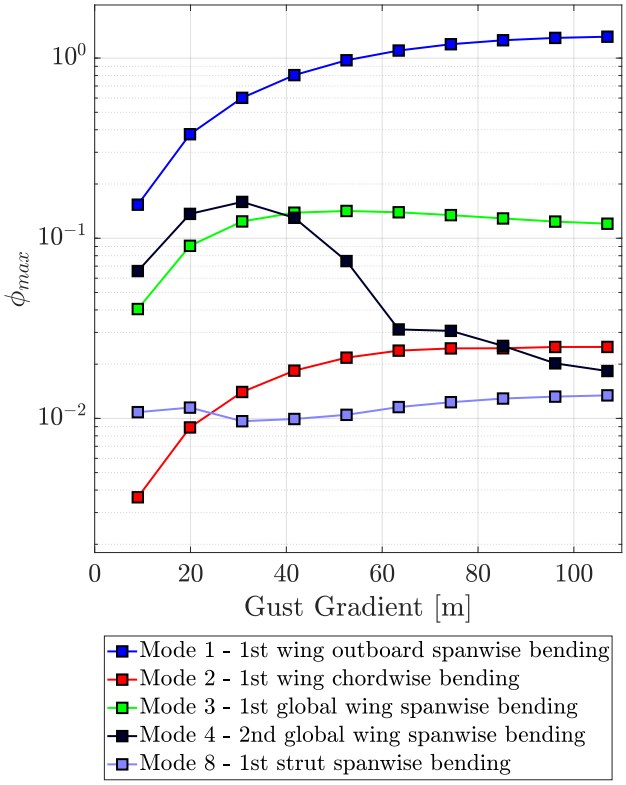

Fig. 7 Maximum modal coordinates as a function of gust gradient

Finally, the relative velocity across the terminals of the jury-strut as a function of gust gradient is shown in Fig. 8. Here, it is shown that the maximum relative velocity is achieved during the 9m gust. This is because the short gusts have the largest bandwidth[38], meaning that they excite the higher frequency modes of the structure which, generally speaking, are truss-dominated modes. Furthermore, due to the higher bandwidth of the short gusts the excitation frequency is much larger which gives a higher velocity and acceleration for a given displacement.[¶]

These results indicate that a vibration suppression device located in parallel with the jury-strut will be particularly effective during the 9m gusts as the input to the device is largest whereas the performance during the longer gusts is likely to be poor due to the considerably lower values of relative velocity acting upon the device. It should be noted that the maximum device stroke across all gust gradients is only 5.3mm. This is clearly not very large and it is possible that if a higher stroke was permissible then a device would provide more of an effect.

[¶]In MSC.Nastran Solution 146 it is assumed that the gust response of the model is harmonic, therefore $\dot{x} = i\omega x$ and $\ddot{x} = -\omega^2 x$.

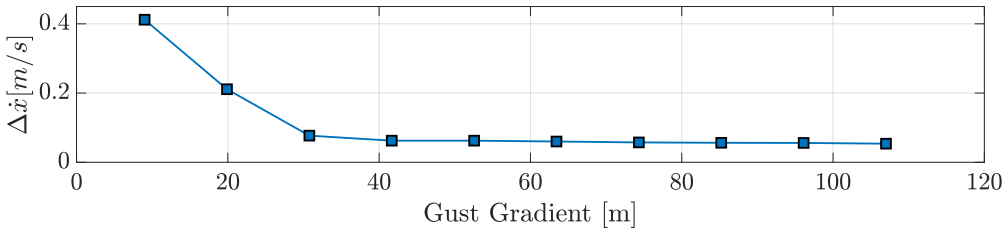

Fig. 8 Relative velocity across the jury-strut terminals vs. gust gradient for the baseline aeroelastic model

V. Gust Loads Alleviation

In this section a vibration suppression device will be located in parallel with the jury-strut element in order to assess the gust loads alleviation potential of this technique. The aim of this section is to assess whether there is a net loads alleviation effect from including an absorber in the truss structure, not to consider the feasibility of such a device. Throughout this study various values for viscous damping coefficient, spring stiffness and inertance have been chosen for the vibration suppression devices. It is important to note that these values have been chosen without any consideration of the physical constraints of the model, for instance, the available space inside the wing box or the maximum available stroke for the device.

In the design of mechanical networks it is common practice to first assess the performance of a single damper element before attempting more complicated layouts as generally the damper represents the simplest possible absorber. This approach is followed in this study, as the performance of the damper will first be evaluated in order to provide a suitable baseline before assessing the performance of the tuned inerter damper.

A. Damper

To assess the loads alleviation effects of the damper in parallel with the jury-strut the gust response of the half-wing model is determined for a range of viscous damping coefficients from $1 \times 10^2 N/ms^{-1}$ to $1 \times 10^5 N/ms^{-1}$.

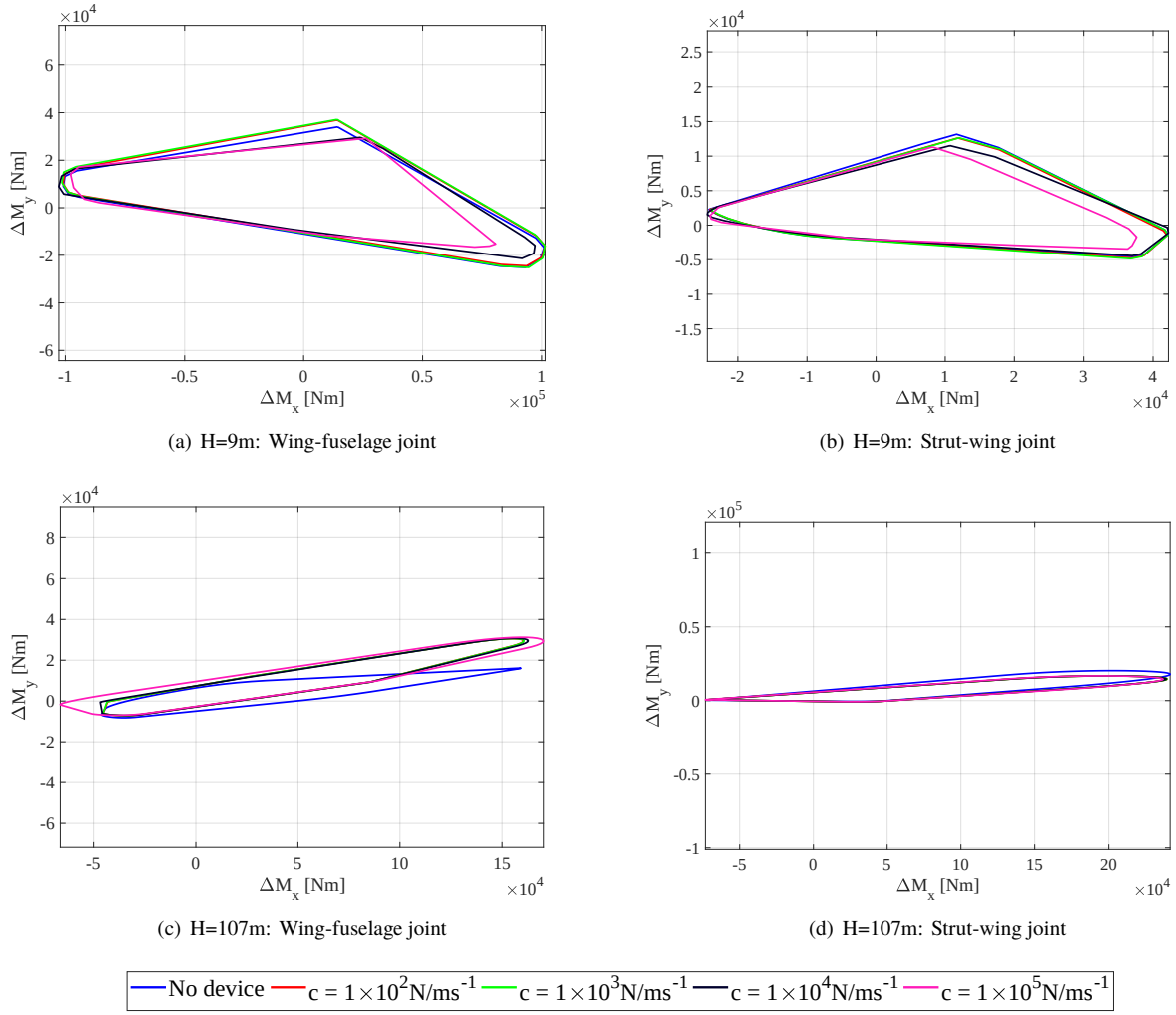

Fig. 9 2D correlated loads plot of torque vs. spanwise bending moment for a range of viscous damping coefficients.

Figure 9 shows the 2D correlated loads diagram for the spanwise bending moment and torque at the wing-fuselage and strut-wing joint for the gust gradients of 9m and 107m.[‖] The wing-fuselage and strut-wing locations have been chosen based on the baseline gust response which indicated that these points along the wing generally exhibit the highest loads.

The results show that, in general, a damper in parallel with the jury-strut can reduce the loads at both locations during a 9m gust, although large values of viscous damping coefficient are required in order provide a net reduction in loads. For the 107m gust, the presence of a damper significantly increases the loads at the wing-fuselage joint and provides only a moderate reduction in loads at the wing-strut joint when compared to the 9m gust results. These observations relate back to the frequency bandwidth of the gust loading and its effect on the input to the device. For the short gusts the higher order truss modes are excited which means that the effects of the absorber are more pronounced, however, for the longer gusts there is less relative motion across the terminals of the device. Further investigation is required to determine why the loads increase at the wing-fuselage joint.

Considering the total loads envelope, Fig. 10 shows that only a very large damping value provides a reduction in spanwise bending moment at the wing root with very little reduction elsewhere along the wing. Furthermore, all values of damping coefficient considered increase the maximum torque at the wing-fuselage joint, something that is clearly not desirable.

In summary, it is clear that the damper can only provide effective loads relief during the shorter gusts, however, as these gusts do not tend to be the critical cases there is limited scope for utilising a damper as a means of loads alleviation. In order to provide a reduction in loads across the entire gust spectrum a device must be considered that can respond to the low frequency excitation of the longer gusts as well as the shorter gusts.

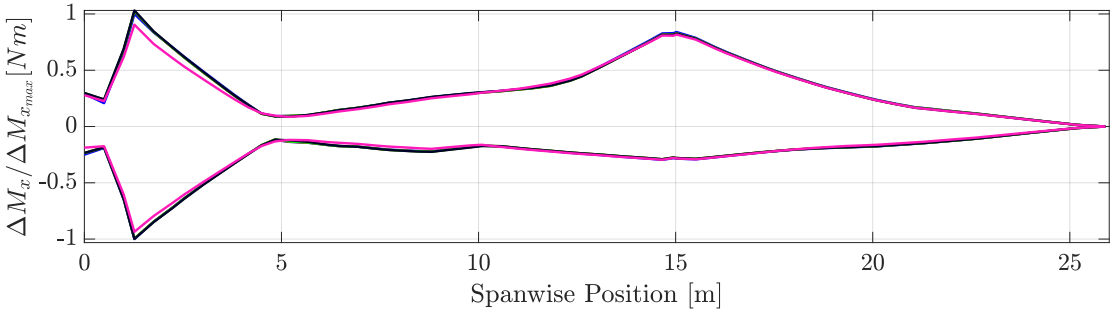

(a) Spanwise bending moment

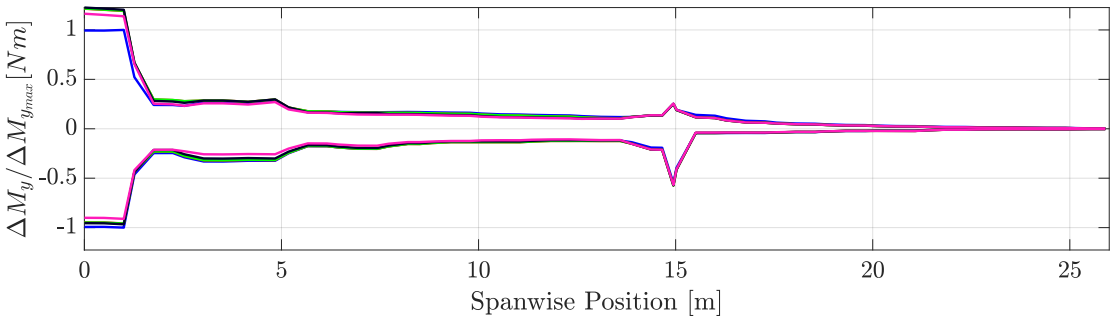

(b) Torque

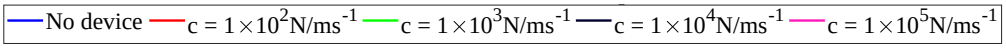

Fig. 10 Normalised incremental loads envelope for the wing using the damper

[‖] In this instance "correlated loads" means correlated with respect to time. To generate these plots a convex hull is fitted to the time domain response of the incremental bending and torque moments.

B. Tuned-Inerter-Damper

In the previous section it was shown that even for large values of viscous damping coefficient a damper element cannot provide consistent loads relief across a broad spectrum of gusts. The main advantage of the tuned inerter damper is the ability to tune the natural frequency of the device in order to target specific vibration modes of the structure, therefore, a TID could be used to target the low frequency modes of the TBW which contribute to most of the critical loads along the wing and the strut elements.

The tuning condition of an absorber located on a flexible structure is a comprehensive subject which considers the background flexibility and inertia effects of the structural modes[39, 40]. Further efforts can be made to tune the damping ratio of the resonant peaks, however these areas are considered beyond the scope of this paper. Instead, the tuning condition for the TID will be taken as

$$\omega_{TID}^2 = \frac{k_{TID}}{b_{TID}}, \tag{10}$$

where ω_{TID} is the tuning frequency, k_{TID} is the spring stiffness and b_{TID} is the inertance value.

The first and second wing bending modes have been selected as candidates for the tuned inerter damper as these modes feature heavily throughout the gust spectrum as shown in Fig. 7. For this initial study, the device inertance and viscous damping coefficient are fixed at $1000kg$ and $1000N/ms^{-1}$respectively. The spring stiffness of the TID is then computed for each tuning frequency using Equation 10.

The results of this study are shown in Fig. 11. The use of a tunable device has enabled a large reduction in bending moment at the wing-fuselage joint with a maximum reduction of 25% for the case when the device is tuned to the second bending mode. Considering the maximum torque loads, the performance of the TID is reduced. Here, the TID actually increases the wing-fuselage torque load when tuned to the first mode but provides a small reduction in loads when tuned to the second bending mode. In both cases there is a significant reduction in minimum torque loads but there is no appreciable effects on the loads towards the wing tip.

Figure 12 shows the modal coordinates for modes 1 and 3 during the 107m gust. These results indicate that tuning the device to the first bending mode actually has little effect on the participation of this mode in the overall gust response.

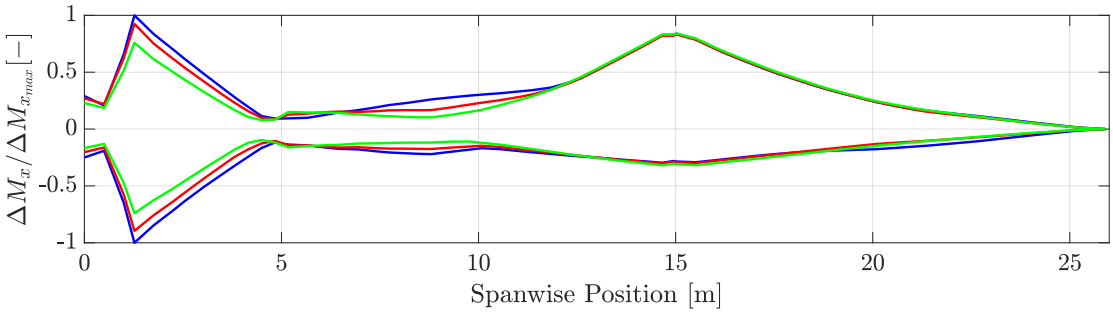

(a) Spanwise bending moment

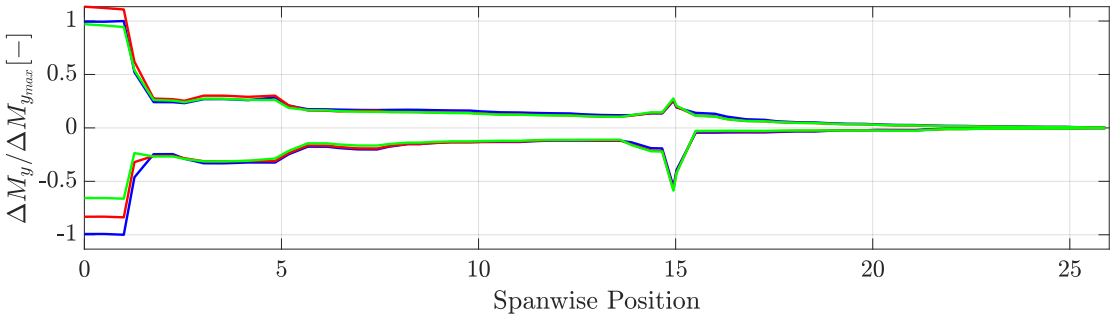

(b) Torque

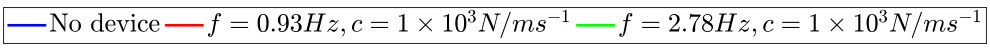

Fig. 11 Normalised incremental loads envelope for the wing using the tuned inerter damper

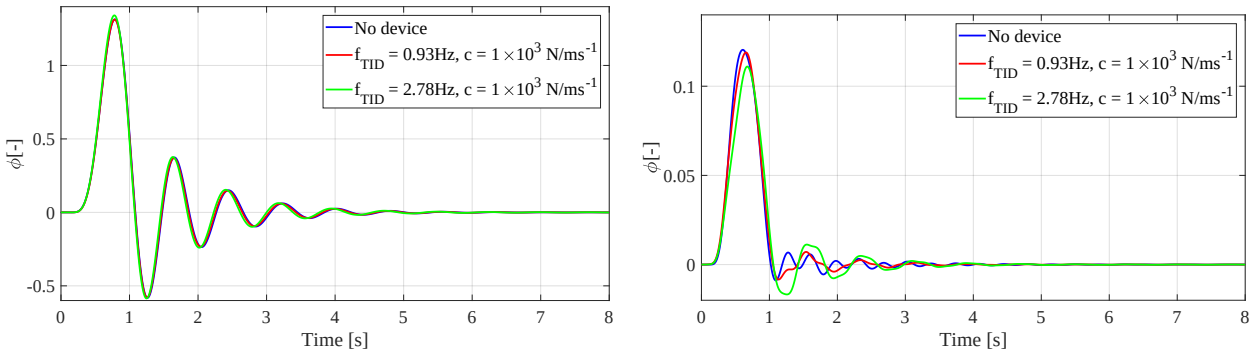

(a) Mode 1 (b) Mode 3

Fig. 12 Modal coordinates for the 107m gust for the different TID tuning parameters

This is because the first mode is almost completely dominated by outboard bending with very little motion exhibited inboard of the strut. This isolated behaviour is facilitated by the pinned-point boundary conditions of the primary strut and it is possible that if a fully-fixed strut connection was implemented the effect of a device may be more pronounced.

For the model considered in this study, it appears that the jury-strut is an inappropriate location for a device that influences the behaviour of the outboard bending mode. It is possible that a rotational device co-located at the strut-wing joint, as in [38], would provide better performance in terms of alleviating the outboard bending.

Finally, it should be noted that the parameter values used for the tuned inerter damper are far smaller than the viscous damping coefficients required for a simple damper device, indicating that a TID may be a more viable layout for the vibration suppression device. Furthermore, the parameter values considered in this study are not optimum meaning that further improvements in terms of gust loads alleviation may be possible.

Overall, implementing a TID in parallel with the jury-strut offers significant benefits to the loads inboard of the strut-wing attachment point. Additional results not presented in this paper have shown that reductions in axial loading and shear force, as well as strut loads, are possible with the use of a tunable device.

VI. Conclusions

This paper has presented a novel method for gust loads alleviation in a truss-braced wing based on using a vibration suppression device located in parallel with the jury-strut to reduce loads across the wing and strut. Two layouts for the vibration suppression device have been considered: a pure damper and a tuned inerter damper.

The results indicated that for the pure damper case very large values of viscous damping coefficient are required in order to provide a reduction in spanwise bending moment at the wing-fuselage joint, however, this is countered by an increase in the torque loads. The tuned inerter damper provided reductions in root bending moment and root torque of 25% and 5% respectively. It is hypothesised that the main driver for the improved performance of the tunable device when compared to the damper is the ability to tune the device to a particular mode of the structure.

Future work will focus on implementing an enhanced tuning condition for the tuned inerter damper device in order to properly account for flexibilty effects and tailor the modal damping ratios. Furthermore, the stiffness of the jury-strut will be investigated to determine whether further reductions in the loads envelope and wing weight are possible by tuning the spring stiffness in order to maximise the performance of the vibration suppression device. Additional applications of a vibration suppression device in truss-braced wings include loads alleviation during continuous turbulence and flutter suppression.

Acknowledgements

This research is funded by UK Aerospace Technology Institute Agile Wing Integration (AWI) project (TSB-113041). Simon A. Neild is supported by an EPSRC Fellowship (EP/K005375/1) and Jason Z. Jiang is supported by an EPSRC grant (EP/P013456/1).

References

[1] Graham, W., Hall, C., and Morales, M. V., "The potential of future aircraft technology for noise and pollutant emissions reduction," *Transport Policy*, Vol. 34, 2014, pp. 36–51.

[2] Sulaeman, E., Kapania, R., and Haftka, R., "Parametric studies of flutter speed in a strut-braced wing," *43rd AIAA/ASME/ASCE/AHS/ASC Structures, Structural Dynamics, and Materials Conference*, 2002, p. 1487.

[3] Bhatia, M., Kapania, R. K., and Haftka, R. T., "Structural and aeroelastic characteristics of truss-braced wings: A parametric study," *Journal of Aircraft*, Vol. 49, No. 1, 2012, pp. 302–310.

[4] Gundlach, J. F., Philippe-André, Té, trault, Gern, F. H., Nagshineh-Pour, A. H., Ko, A., Schetz, J. A., Mason, W. H., Kapania, R. K., et al., "Conceptual design studies of a strut-braced wing transonic transport," *Journal of aircraft*, Vol. 37, No. 6, 2000, pp. 976–983.

[5] Meadows, N. A., Schetz, J. A., Kapania, R. K., Bhatia, M., and Seber, G., "Multidisciplinary design optimization of medium-range transonic truss-braced wing transport aircraft," *Journal of Aircraft*, Vol. 49, No. 6, 2012, pp. 1844–1856.

[6] Green, J., "Laminar flow control-back to the future?" *38th Fluid Dynamics Conference and Exhibit*, 2008, p. 3738.

[7] Philippe-André, Té, trault, Schetz, J. A., and Grossman, B., "Numerical prediction of interference drag of strut-surface intersection in transonic flow," *AIAA journal*, Vol. 39, No. 5, 2001, pp. 857–864.

[8] Duggirala, R. K., Roy, C. J., and Schetz, J. A., "Analysis of interference drag for strut-strut interaction in transonic flow," *AIAA journal*, Vol. 49, No. 3, 2011, pp. 449–462.

[9] Carrier, G., Atinault, O., Dequand, S., Hantrais-Gervois, J., Liauzun, C., Paluch, B., Rodde, A., and Toussaint, C., "Investigation of a strut-braced wing configuration for future commercial transport," *28th Congress of the International Council of the Aeronautical Sciences*, ICAS Bonn, 2012, pp. 2012–1.

[10] Mallik, W., Kapania, R. K., and Schetz, J. A., "Effect of flutter on the multidisciplinary design optimization of truss-braced-wing aircraft," *Journal of Aircraft*, Vol. 52, No. 6, 2015, pp. 1858–1872.

[11] Bradley, M. K., and Droney, C. K., "Subsonic Ultra Green Aircraft Research: Phase I Final Report," Tech. rep., NASA, CR-2011-216847, 2011.

[12] Bradley, M. K., Droney, C. K., and Allen, T. J., "Subsonic Ultra Green Aircraft Research. Phase II-Volume I; Truss Braced Wing Design Exploration," Tech. rep., NASA, CR-2015-218704, 2015.

[13] Karpel, M., "Design for active flutter suppression and gust alleviation using state-space aeroelastic modeling," *Journal of Aircraft*, Vol. 19, No. 3, 1982, pp. 221–227.

[14] Bradley, M. K., Allen, T. J., and Droney, C., "Subsonic Ultra Green Aircraft Research: Phase II-Volume III; Truss Braced Wing Aeroelastic Test Report," Tech. rep., NASA, CR-2015-218704, 2014.

[15] Castrichini, A., Siddaramaiah, V. H., Calderon, D., Cooper, J., Wilson, T., and Lemmens, Y., "Preliminary investigation of use of flexible folding wing tips for static and dynamic load alleviation," *The Aeronautical Journal*, Vol. 121, No. 1235, 2017, pp. 73–94.

[16] Stodieck, O., Cooper, J. E., Weaver, P., and Kealy, P., "Optimization of tow-steered composite wing laminates for aeroelastic tailoring," *AIAA Journal*, Vol. 53, No. 8, 2015, pp. 2203–2215.

[17] Wlezien, R., Horner, G., McGowan, A., Padula, S., Scott, M., Silcox, R., and Simpson, J., "The aircraft morphing program," *39th AIAA/ASME/ASCE/AHS/ASC Structures, Structural Dynamics, and Materials Conference and Exhibit*, 1998, p. 1927.

[18] Haskett, T., Breukelman, B., Robinson, J., and Kottelenberg, J., "Tuned-Mass Damper Under Excessive Structural Excitation," *Report of the Motioneering Inc., Guelph, Ontario, Canada*, 2004.

[19] Smith, M. C., "Synthesis of mechanical networks: The inerter," *IEEE Transactions on Automatic Control*, Vol. 47, No. 10, 2002, pp. 1648–1662.

[20] Jiang, J. Z., and Smith, M. C., "Regular positive-real functions and five-element network synthesis for electrical and mechanical networks," *IEEE Transactions on Automatic Control*, Vol. 56, No. 6, 2011, pp. 1275–1290.

[21] Smith, M. C., and Wang, F.-C., "Performance benefits in passive vehicle suspensions employing inerters," *Vehicle System Dynamics*, Vol. 42, No. 4, 2004, pp. 235–257.

[22] Jiang, J. Z., Matamoros-Sanchez, A. Z., Goodall, R. M., and Smith, M. C., "Passive suspensions incorporating inerters for railway vehicles," *Vehicle System Dynamics*, Vol. 50, No. sup1, 2012, pp. 263–276.

[23] Jiang, J., Matamoros-Sanchez, A., Zolotas, A., Goodall, R., and Smith, M., "Passive suspensions for ride quality improvement of two-axle railway vehicles," *Proceedings of Mechanical Engineering Part F: Journal of Rail and Rapid Transit*, Vol. 229, No. 3, 2015, pp. 315–329.

[24] Lazar, I., Neild, S., and Wagg, D., "Using an inerter-based device for structural vibration suppression," *Earthquake Engineering & Structural Dynamics*, Vol. 43, No. 8, 2014, pp. 1129–1147.

[25] Zhang, S. Y., Jiang, J. Z., and Neild, S., "Optimal configurations for a linear vibration suppression device in a multi-storey building," *Structural Control and Health Monitoring*, 2016.

[26] Li, Y., Jiang, J. Z., and Neild, S., "Inerter-Based Configurations for Main-Landing-Gear Shimmy Suppression," *Journal of Aircraft*, 2016, pp. 1–10.

[27] Li, Y., Jiang, J. Z., Neild, S. A., and Wang, H., "Optimal Inerter-Based Shock–Strut Configurations for Landing-Gear Touchdown Performance," *Journal of Aircraft*, 2017.

[28] Zhang, S. Y., Jiang, J. Z., and Neild, S. A., "Passive vibration control: a structure–immittance approach," *Proceedings of the Royal Society of London A: Mathematical, Physical and Engineering Sciences*, Vol. 473, No. 2201, 2017. doi:10.1098/rspa.2017.0011, URL `http://rspa.royalsocietypublishing.org/content/473/2201/20170011`.

[29] Szczyglowski, C. P., Howcroft, C., Neild, S. A., Titurus, B., Jiang, J. Z., Cooper, J. E., and Coetzee, E., "Strut-Braced Wing Modelling with a Reduced Order Beam Model," *Proceedings of the Royal Aeronautical Engineering Society 5th Aircraft Structural Design Conference, Manchester, United Kingdom*, 2016.

[30] Hart-Smith, L., "The ten-percent rule for preliminary sizing of fibrous composite structures," *Weight Engineering*, Vol. 52, 1992, pp. 29–45.

[31] Haftka, R. T., and Gürdal, Z., *Elements of structural optimization*, Vol. 11, Springer Science & Business Media, 2012.

[32] Su, W., "Nonlinear Aeroelastic Analysis of Aircraft with Strut-Braced Highly Flexible Wings," *58th AIAA/ASCE/AHS/ASC Structures, Structural Dynamics, and Materials Conference*, 2017, p. 1351.

[33] *CS-25 Certification Specifications for Large Aeroplanes*, European Aviation Safety Agency (EASA), 2003.

[34] Guillemin, E. A., *Synthesis of passive networks: theory and methods appropriate to the realization and approximation problems*, Wiley, 1957.

[35] Gonzalez-Buelga, A., Lazar, I. F., Jiang, J. Z., Neild, S. A., and Inman, D. J., "Assessing the effect of nonlinearities on the performance of a tuned inerter damper," *Structural Control and Health Monitoring*, Vol. 24, No. 3, 2017.

[36] McCormick, C. W., *MSC/NASTRAN User's Manual: MSC/NASTRAN Version 63*, MacNeal-Schwendler Corporation, 1983.

[37] Gockel, M., *MSC/NASTRAN Handbook for Dynamic Analysis: MSC/NASTRAN Version 63*, MacNeal-Schwendler Corporation, 1983.

[38] Szczyglowski, C. P., Neild, S. A., Titurus, B., Jiang, J. Z., Cooper, J. E., and Coetzee, E., "Passive Gust Loads Alleviation in a Truss-Braced Wing Using Integrated Dampers," *Proceedings of the 17th International Forum on Aeroelasticity and Structural Dynamics, Como, Italy*, 2017.

[39] Krenk, S., and Høgsberg, J., "Tuned mass absorber on a flexible structure," *Journal of Sound and Vibration*, Vol. 333, No. 6, 2014, pp. 1577–1595.

[40] Krenk, S., and Høgsberg, J., "Tuned resonant mass or inerter-based absorbers: unified calibration with quasi-dynamic flexibility and inertia correction," *Proc. R. Soc. A*, Vol. 472, The Royal Society, 2016, p. 20150718.